Structure and dielectric properties of ferroelectric pyridinium perrhenate crystals

2000 J. Phys.: Condens. Matter 12 4881

(http://iopscience.iop.org/0953-8984/12/22/319)

J. Phys.: Condens. Matter **12** (2000) 4881–4892. Printed in the UK PII: S0953-8984(00)11986-1

Structure and dielectric properties of ferroelectric pyridinium perrhenate crystals

P Czarnecki and H Małuszyńska

Faculty of Physics, Adam Mickiewicz University, Umultowska 85, 61-614 Poznań, Poland

E-mail: pczarnec@main.amu.edu.pl (P Czarnecki)

Received 21 February 2000

Abstract. The crystal and molecular structure of a new ferroelectric $[C_5H_6N]^+ReO_4^-$ was determined by the x-ray diffraction method at 350 K, 293 K and 220 K. In all three phases its structure is orthorhombic, with the following sequence of space groups: $Cmcm \overset{336\ K}{\Longrightarrow} Cmc2_1 \overset{250\ K}{\Longrightarrow} Pbca$. In the two high-temperature phases, the pyridinium cations are disordered while the anions are ordered. The low-temperature phase is fully ordered.

The complex permittivity of a ferroelectric single crystal of pyridinium perrhenate was measured in the frequency range from 1 kHz to 13 MHz. The results confirm the order–disorder nature of the continuous ferroelectric phase transition at $T_1 = 336$ K. In the vicinity of the ferroelectric phase transition, the phenomenon of critical slowing down was detected. The dielectric relaxation in the paraelectric phase can be described by the Debye relaxation equation with a single relaxation time. The nature of the ferroelectricity is related to the degree of disorder of the pyridinium cation as well as to the appearance and the alignment of the dipole moment of the ReO_4^- anion.

1. Introduction

The recently discovered ferroelectric properties of such pyridinium salts as pyridinium tetrafluoroborate ($PyBF_4$) [1] and pyridinium perchlorate ($PyClO_4$) [2] have aroused new interest in this group of compounds, which has resulted in the identification of two other ferroelectric crystals: pyridinium perrhenate (denoted as $PyReO_4$) [3] and pyridinium periodide ($PyIO_4$) [4]. Both of these new ferroelectrics are of special interest because their Curie temperatures are above room temperature [5]. Many pyridinium salts are known to undergo phase transitions; however, ferroelectric phase transitions have been discovered only in salts with the monovalent tetrahedral anions BF_4^-, ClO_4^-, IO_4^- and ReO_4^-. The ferroelectric properties of pyridinium salts are related to the disorder of the pyridinium cation and to some distortions from the ideal tetrahedral symmetry of the anion. NMR studies of pyridinium salts [6–9] revealed that cations and tetrahedral anions perform fast reorientations in high-temperature phases causing disorder of the crystal structures. All of the ferroelectric and non-ferroelectric pyridinium salts already discovered crystallize in the trigonal system in disordered high-temperature phases with only one structural unit (with $Z = 1$) in the elementary cell—e.g. $PyBF_4$ [10], $PyClO_4$ [9], PyI [11]. For none of these salts has a ferroelectric phase been fully determined by the x-ray diffraction method because of the multidomain structure. $PyReO_4$ (and isostructural $PyIO_4$) are the first pyridinium salts which crystallize in the orthorhombic system in the ferroelectric room temperature phase [3, 12]. According to the results of preliminary dielectric studies on

0953-8984/00/224881+12$30.00

polycrystalline samples [3], $PyReO_4$ undergoes a continuous ferroelectric phase transition at 333 K and a discontinuous non-ferroelectric one at 250 K. It is interesting to check whether $PyReO_4$ belongs to the unique group of multiaxial ferroelectrics undergoing a continuous phase transition [10], like $PyBF_4$ crystal.

In this paper we present x-ray diffraction investigations of $PyReO_4$ monocrystals at 350 K, 293 K and 220 K and dielectric spectroscopy studies. The nature of the ferroelectricity of pyridinium perrhenate is also discussed.

2. Experimental procedure

The pyridinium perrhenate salt was prepared by allowing the pyridinium base dissolved in 50% ethanol to react with perrhenic acid obtained by dissolving rhenium oxide in water. The substance obtained in this way was recrystallized three times. $PyReO_4$ monocrystals were grown from water solution by slow evaporation at a constant temperature of 300 K.

X-ray data were collected on a KM-4 KUMA diffractometer with Mo Kα radiation ($\lambda = 0.710\,72$ Å), and on a graphite monochromator by the ω–2Θ scan technique at 293 K and 350 K. The data at 220 K were collected using a KUMA CCD camera.

The cycles of cooling down and heating were carried out at 120 K h^{-1} using an Oxford Cryosystem. The cell dimensions of the two high-temperature phases were refined from setting the angles of 35 reflections in the range $15^\circ < 2\Theta < 30^\circ$. A summary of the crystal data and structure refinements is given in table 1. The Lorentz polarization and semi-empirical absorption corrections were applied.

Table 1. Crystal data and structure refinement for $[C_5H_6N]^+ReO_4^-$ at 220 K, 293 K and 350 K.

Temperature	220 K	293 K	350 K
Formula weight	330.3	330.3	330.3
Crystal system	*Pbca*	$Cmc2_1$	*Cmcm*
Unit cell (Å)	$a = 16.994(3)$	8.377(2)	8.390(2)
	$b = 7.208(1)$	7.285(1)	7.346(1)
	$c = 12.084(2)$	12.391(2)	12.445(2)
Volume ($Å^3$)	1480.2(4)	756.2(2)	767.0(2)
Wavelength (Å)	0.71073	0.71073	0.71073
Z, density (Mg m^{-3})	8, 2.964	4, 2.901	4, 2.860
Absorption (mm^{-1})	16.382	16.034	15.807
Crystal size (mm)	$0.15 \times 0.07 \times 0.1$	$0.15 \times 0.2 \times 0.2$	$0.15 \times 0.2 \times 0.2$
Theta range (deg)	2.40 to 29.42	3.29 to 24.94	3.29 to 24.94
Reflections collected, unique, R(int)	8969, 1944, 0.077	707, 707, 0.12	962, 380, 0.12
Refinement method	Full-matrix least squares on F2		
Data/restraints/parameters	944/0/97	707/0/55	380/0/31
Goodness of fit on F2	1.240	1.050	1.192
Final R-indices $I > 2\sigma(I)$	$R_1 = 0.0782$	$R_1 = 0.0292$	$R_1 = 0.0369$
	$wR_2 = 0.2247$	$wR_2 = 0.0738$	$wR_2 = 0.0933$
Largest difference, peak and hole (e $Å^{-3}$)	7.90 and −7.02	0.52 and −1.34	1.55 and −1.99

Complex permittivity measurements were performed for a few frequencies from 1 kHz to 13 MHz using an impedance analyser, HP-4192A, from Hewlett-Packard. Dielectric measurements were carried out at temperatures from 310 to 350 K at a rate of temperature change of 0.02 K min^{-1} near the phase transition and of 0.5 K min^{-1} far away from it. The measurements were performed using a sample of size $2 \times 2 \times 1$ mm in the direction of the twofold polar axis of the orthorhombic system. We did not perform dielectric measurements below 310 K to avoid breaking the large monocrystal at the strong first-order phase transition at 250 K. The breaking did not occur for the very small monocrystals used for x-ray measurements. The measuring ac electric field was of about 2 V cm^{-1}.

3. Results and discussion

3.1. X-ray measurements

The structures of the three phases were resolved by the Patterson method using SHELXS-86 [13] and refined anisotropically by the full-matrix least-squares method using SHELXL-98 [14].

The positions of all non-hydrogen atoms were found from the peaks on the difference Fourier map; the hydrogen-atom positions were calculated theoretically assuming a C–H distance of 1.09 Å and an N–H distance of 1.03 Å. The high-temperature phase at 350 K has been refined in the $Cmcm$ space group to $R = 0.037$. The pyridinium cation is disordered and reveals mm symmetry. Therefore the N-atom position cannot be determined, and all pyridinium ring atoms were assumed to be carbons. The ReO_4^- anion is ordered and displays mm symmetry.

The atomic coordinates and equivalent isotropic temperature factors are given in table 2(a), whereas the bond distances and angles appear in table 3(a). The geometrical parameters of the cation and anion, such as bond lengths and angles, agree well within experimental errors with their expected values.

The room temperature phase loses the centre of symmetry and has been refined in the $Cmc2_1$ space group to the R-factor of 0.029. At the end of the least-squares refinement, the racemic twinning model was introduced, giving a better convergence with the Flack [15] absolute-structure x-parameter of 0.45(9). The pyridinium cation as well as the ReO_4^- anion preserve only one mirror plane. The pyridinium cation is disordered with the mirror plane going through the centre of two C–C bonds and through Re, O(1), O(2) and O(3) atoms in ReO_4^-.

Because the bond lengths and angles were poorly resolved (see table 3(b)) we have also refined the structure in the room temperature phase in the centrosymmetric space group $Cmcm$. The convergence and the molecular geometry improved significantly but the centrosymmetric model had to be rejected because of the ferroelectric properties of this phase. The better convergence of the centrosymmetric model may be a consequence of the pseudo-symmetry generated by the positions of the Re ($Z = 75$) atoms being related to each other through a pseudo-centre of symmetry or to the existence of racemic twinning.

The low-temperature phase at 220 K is ordered and has been refined in the $Pbca$ space group with the unit-cell parameter a doubled with respect to that in the room temperature phase. There are eight $PyReO_4$ in the unit cell and all atoms in the cation and the anion are symmetrically independent. The nitrogen-atom position has been located on the difference Fourier map.

The refinement converged at $R = 0.078$ and all other possible space groups, non-centrosymmetric ones included, failed to give better convergence. The bond lengths and valency angles in ReO_4^- are greater than in the high-temperature phase (see table 3) due to

Table 2. Atomic coordinates ($\times 10^4$) and equivalent isotropic displacement parameters ($\times 10^3$ Å^2) for $PyReO_4$ at (a) 350 K; (b) 293 K; (c) 220 K. U(eq) is defined as one third of the trace of the orthogonalized U_{ij}-tensor; o.f. is an occupancy factor.

	x/a	y/b	z/c	U(eq)	o.f.
(a) 350 K					
Re	0	8537 (1)	2500	47 (1)	0.25
O(1)	0	9868 (29)	3598 (17)	122 (7)	0.5
O(2)	−1639 (16)	7228 (25)	2500	96 (5)	0.5
C(1)	785 (19)	3974 (14)	4292 (12)	69 (3)	1.0
C(2)	1628 (21)	5000	5000	73 (5)	0.5
H(1)	1413 (19)	3122 (14)	3713 (12)	80	1.0
H(2)	2927 (21)	5000	5000	80	0.50
(b) 293 K					
Re	0	8532 (1)	0	36 (1)	0.5
O(1)	0	9550 (80)	1290 (30)	100 (10)	0.5
O(2)	−1663 (14)	7212 (16)	−160 (40)	77 (7)	1.0
O(3)	0	10080 (60)	−940 (30)	86 (12)	0.5
C(1)	740 (50)	3840 (50)	1780 (30)	41 (8)	1.0
C(2)	1632 (17)	4940 (80)	2470 (40)	57 (5)	1.0
C(3)	880 (40)	5850 (50)	3200 (30)	51 (10)	1.0
H(1)	1350	2944	1204	60	1.0
H(2)	1552	6627	3801	60	1.0
H(3)	2927	4982	2392	60	1.0
(c) 220 K					
Re	1364 (1)	8843 (1)	−2374 (1)	21 (1)	1.0
O(1)	593 (8)	10386 (19)	−2623 (10)	31 (3)	1.0
O(2)	2270 (7)	9841 (17)	−2802 (10)	29 (3)	1.0
O(3)	1421 (8)	8390(20)	−968 (10)	52 (5)	1.0
O(4)	1200 (8)	6780 (20)	−3057 (16)	46 (4)	1.0
C(1)	705 (11)	1570 (30)	662 (16)	32 (4)	1.0
C(2)	371 (12)	2610 (20)	−138 (14)	29 (4)	1.0
C(3)	839 (12)	3730 (20)	−804 (15)	29 (4)	1.0
C(4)	1652 (10)	3750 (20)	−638 (14)	25 (4)	1.0
C(5)	1971 (10)	2660 (20)	204 (13)	25 (4)	1.0
N	1497 (10)	1550 (20)	827 (14)	34 (4)	1.0
H(1)	327	748	1203	30	1.0
H(2)	−262	2545	−278	30	1.0
H(3)	576	4591	−1444	30	1.0
H(4)	2034	4604	−1153	30	1.0
H(5)	2602	2700	368	30	1.0
H(6)	1734	688	1414	30	1.0

Table 3. Bond lengths (Å) and valency angles (deg) in $PyReO_4$ at (a) 350 K; (b) 293 K; (c) 220 K. (The symmetry transformations used to generate equivalent atoms at 350 K and 293 K are: superscript a: $x, y, -z + 1/2$; superscript b: $-x, y, z$; superscript c: $-x, y, -z + 1/2$; superscript d: $x, -y + 1, -z + 1$.)

Bond	Length (Å)	Atoms	Angle (deg)
(a) 350 K			
Re–O(1)	1.68 (2)	O(1)–Re–O(1)[a]	109 (2)
Re–O(2)	1.678 (13)	O(1)–Re–O(2)	109.5 (6)
C(1)–C(1)[b]	1.32 (3)	O(2)–Re–O(2)[c]	110.1 (13)
C(1)–C(2)	1.36 (2)	C(1)[b]–C(1)–C(2)	121.4 (9)
		C(1)–C(2)–C(1)[d]	117 (2)
(b) 293 K			
Re–O(1)	1.76 (4)	O(1)–Re–O(2)	110.1 (17)
Re–O(2)	1.705 (12)	O(1)–Re–O(3)	110.9 (17)
Re–O(3)	1.62 (3)	O(2)–Re–O(2)[b]	109.7 (10)
C(1)–C(1)[b]	1.24 (8)	O(3)–Re–O(2)[b]	108.0 (16)
C(1)–C(2)	1.40 (7)	O(3)–Re–O(2)	108.0 (16)
C(2)–C(3)	1.28 (7)	O(1)–Re– O(2)[b]	110.1 (17)
C(3)–C(3)[b]	1.48 (7)	C(1)[b]–C(1)–C(2)	122.3 (18)
		C(2)–C(3)–C(3)[b]	119.4 (19)
		C(1)–C(2)–C(3)	118.0 (15)
(c) 220 K			
Re–O(1)	1.744 (13)	O(1)–Re–O(2)	110.0 (6)
Re–O(2)	1.776 (12)	O(1)–Re–O(3)	109.4 (7)
Re–O(3)	1.734 (18)	O(1)–Re–O(4)	110.2 (7)
Re–O(4)	1.722 (16)	O(2)–Re–O(3)	108.3 (6)
C(1)–N	1.36 (3)	O(2)–Re–O(4)	110.5 (7)
C(1)–C(2)	1.35 (3)	O(3)–Re–O(4)	108.3 (8)
C(2)–C(3)	1.39 (3)	N–C(1)–C(3)	121.9 (18)
C(3)–C(4)	1.40 (2)	C(1)–C(2)–C(3)	119.7 (19)
C(4)–C(5)	1.39 (2)	C(2)–C(3)–C(4)	119.4 (16)
C(5)–N	1.37 (2)	C(3)–C(4)–C(5)	118.9 (15)
		C(4)–C(5)–N	120.3 (17)
		C(5)–N–C(1)	119.8 (16)

much lower temperature factors. The Re–O bond lengths differ and are in the range of 1.720(16) to 1.775(12) Å, while the O–Re–O angles are closer to their expected values (with a mean value of 109.4°). The C–C and C–N bond lengths are rather equal within 2σ, and from the geometry of the pyridinium cation it is impossible to determine the position of the N atom.

The Ortep drawings at 50% probability of $PyReO_4$ in three phases are given in figures 1(a), 1(b), 1(c).

The pyridinium cations form layers parallel to the x-axis interconnected with ReO_4^- anions. The cation's layers make an angle of about 45° with the z-axis (see figure 2). Because of the disorder of the pyridinium cation in the two high-temperature phases, the only intermolecular interactions are the C–H$\cdots$O ones, which may be considered as weak bifurcated hydrogen bonds [16].

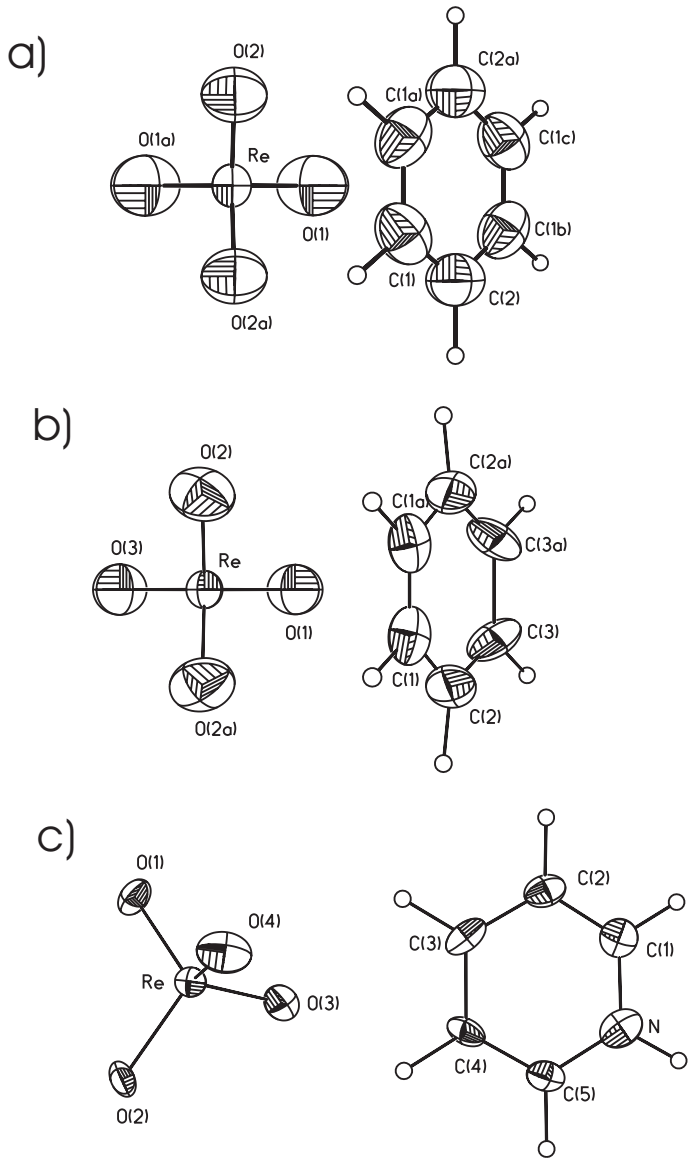

Figure 1. The Ortep drawings at 50% probability of $PyReO_4$ at (a) 350 K, (b) 293 K and (c) 220 K.

The C···O distances range from 3.206 Å to 3.359 Å at 350 K and from 3.194 Å to 3.448 Å for the room temperature phase. Each hydrogen atom acts as a double donor and the second component of the bifurcated hydrogen bond interconnects the perrhenate ions with each other along the *y*-axis.

In the low-temperature phase the N–H···O hydrogen bond is well defined as bifurcated with H···O(2) and H···O(4) distances of 1.97 Å and 2.10 Å, angles N–H···O(2) of 142° and N–H···O(4) of 123° and N···O(2) and N···O(4) distances of 2.854 Å and 2.799 Å respectively. The remaining C···O distances are significantly longer and they range from 2.990 Å to 3.498 Å.

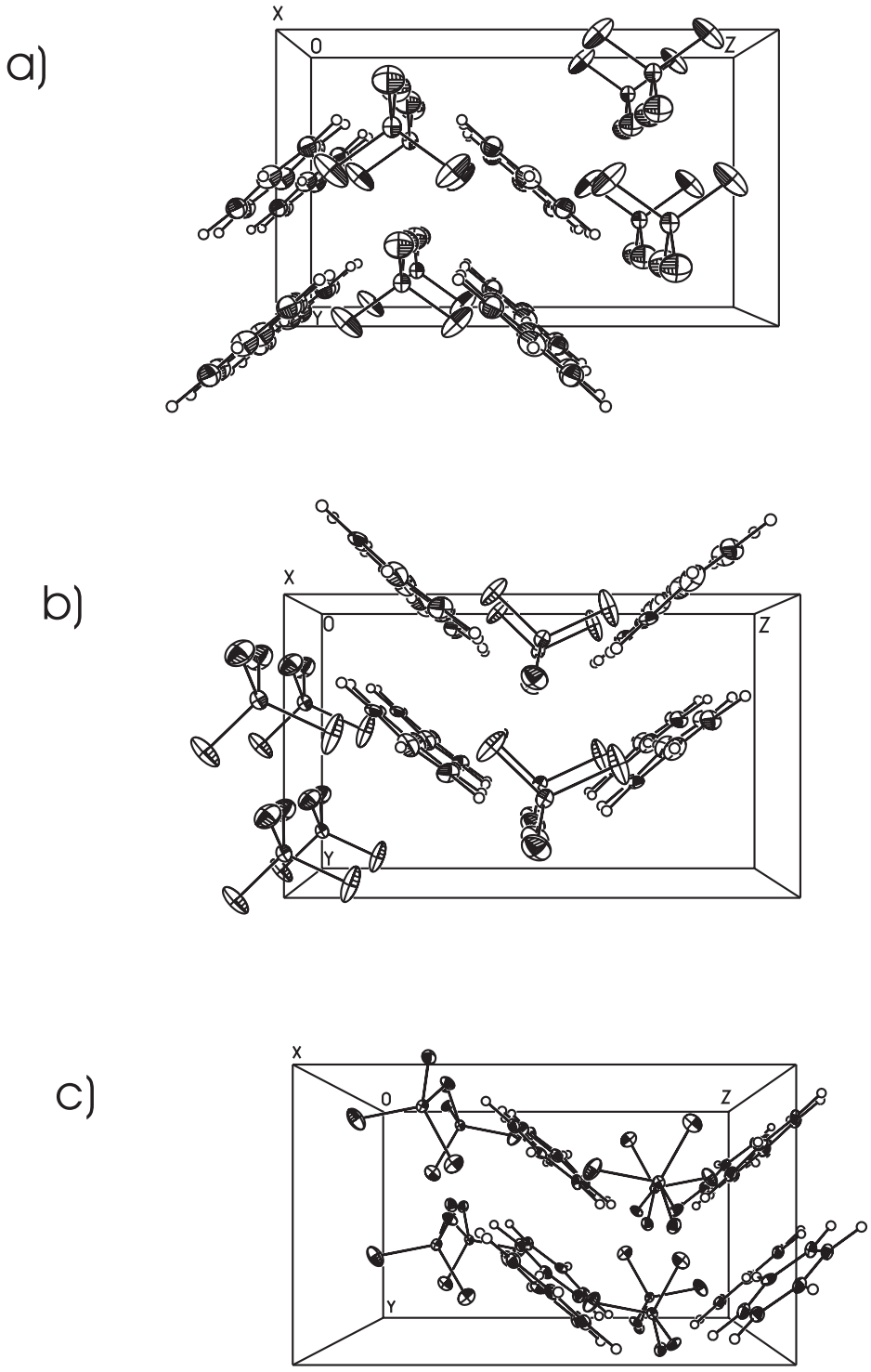

Figure 2. The packing arrangement in three phases at (a) 350 K, (b) 293 K (two unit cells) and at (c) 220 K (one unit cell) in the *yz*-plane.

There are almost no changes in the packing arrangement in all three phases (see figures 2(a), 2(b), 2(c)), except that the packing becomes more symmetrical going from the lower- to the higher-symmetry space group.

3.2. Dielectric measurements

The results of permittivity and loss tangent (tan δ) measurements are presented in figures 3(a) and 3(b). At low frequencies, the permittivity ϵ' reaches a maximum at $T_1 = 336$ K and its temperature dependence is typical of the continuous ferroelectric phase transition. To verify the continuous character of the phase transition we analysed the temperature dependence of the inverse permittivity, shown in figure 4. It is linear and does not reveal any discontinuities near the Curie point. The temperature dependence of the inverse permittivity is linear and the slope is different for the ferroelectric and paraelectric phases. The Curie–Weiss constants estimated from figure 4 are $C_+ = 1375$ K in the paraelectric phase and $C_- = 525$ K in the ferroelectric phase. These values are typical of the order–disorder-type ferroelectrics. The ratio of the Curie–Weiss constants in the paraelectric and ferroelectric phases is $C_+/C_- = 2.6$, which is slightly higher than 2, predicted theoretically for second-order phase transitions. To estimate this ratio we chose as the measuring ac frequency not 1 kHz (the lowest) but 100 kHz, to reduce the effect of dielectric dispersion in the ferroelectric phase due to the domain-wall motion on the slope of the inverse permittivity in the ferroelectric phase. The slope value of 2.6 is similar to the value measured for TGS [17] crystals, which are usually considered as typical examples of ferroelectrics with the continuous phase transition.

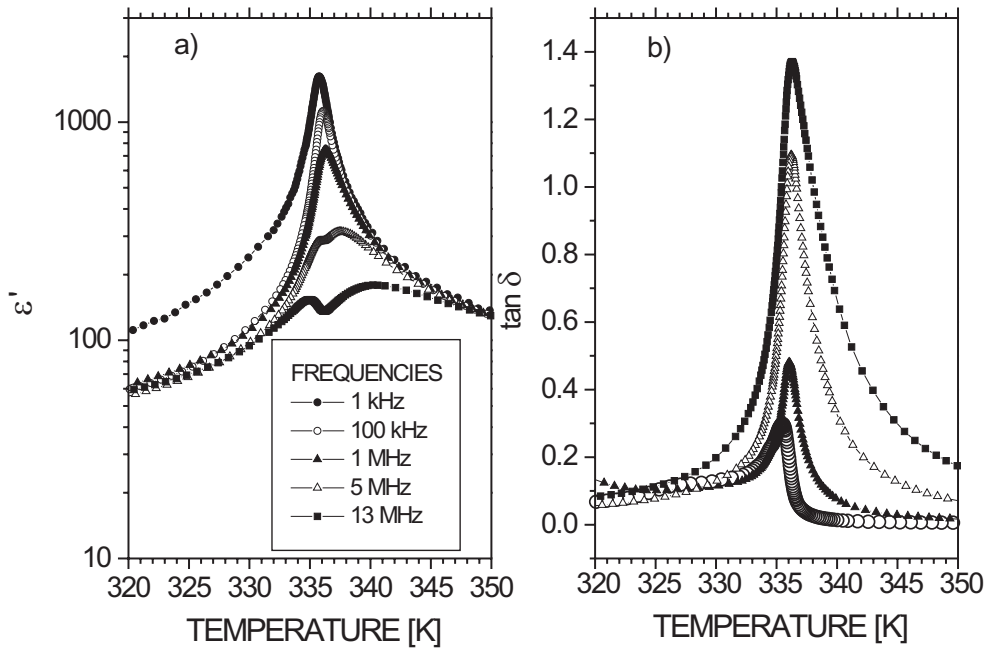

Figure 3. Permittivity (a) and loss tangent tan δ (b) in the vicinity of the ferroelectric phase.

At higher frequencies, the permittivity shows a minimum at the Curie point $T_1 = 336$ K and two broad maxima below and above T_1 (figure 3(a)). The temperature dependence of tan δ reveals a sharp maximum whose value increases with increasing frequency of the measuring

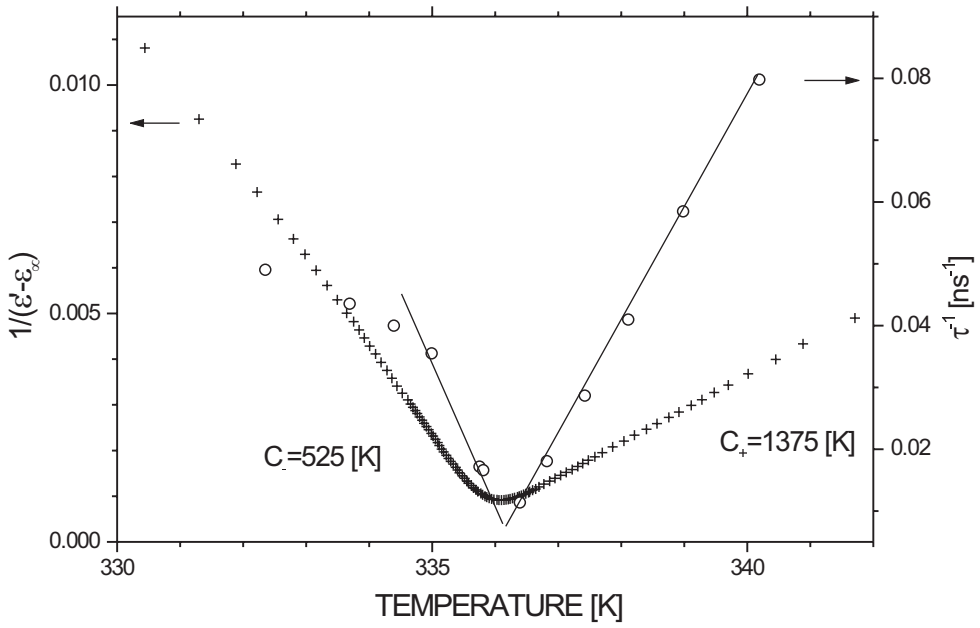

Figure 4. The temperature dependence of the inverse relaxation time τ^{-1} (right-hand scale) and inverse permittivity for 100 kHz (left-hand scale).

field (figure 3(b)). Such a temperature dependence of $\tan\delta$ and the permittivity is known as the critical slowing down.

Figure 5 presents the Cole–Cole plots in the paraelectric phase (a) and the ferroelectric phase (b) for a few temperatures close to the ferroelectric Curie point. In the paraelectric phase the shape of the Cole–Cole plot suggests an almost monodispersive character of the permittivity whose frequency dependence can be described by the equation

$$\epsilon^* = \epsilon_\infty + \frac{\epsilon_0 - \epsilon_\infty}{1 + (\mathrm{i}\omega\tau)^{1-\alpha}} \tag{1}$$

where ϵ_0 and ϵ_∞ are the static and high-frequency values of the permittivity. The fitted α-values are of about 0.08 for $T - T_c$ equal to 0.82 K and 1.42 K. Close to the Curie point ($T - T_c$ equal to 0.39 K), $\alpha = 0.21$, which means that some polydispersity appears very close to the Curie point. In the ferroelectric phase—figure 5(b)—there are two relaxational processes. One is related to the critical slowing down and the other to dielectric dispersion due to the domain-wall motion [18]. The critical slowing is a result of the relaxation of fluctuation in the order parameter described by the Khalatnikov–Landau equation [19]. The relaxation time critically depends on temperature:

$$\tau \sim (T - T_c)^{-1}. \tag{2}$$

Equation (2) could be written in a more convenient form:

$$\tau = \frac{\tau_0 T_c}{T - T_c} \tag{3}$$

where τ_0 is a relaxation time characteristic of the critical slowing down. Figure 4 presents the temperature dependence of the inverse relaxation time τ^{-1}. Above the Curie temperature $T_1 = 336$ K, τ^{-1} is well fitted with equation (3), while below T_1, the non-linear dependence

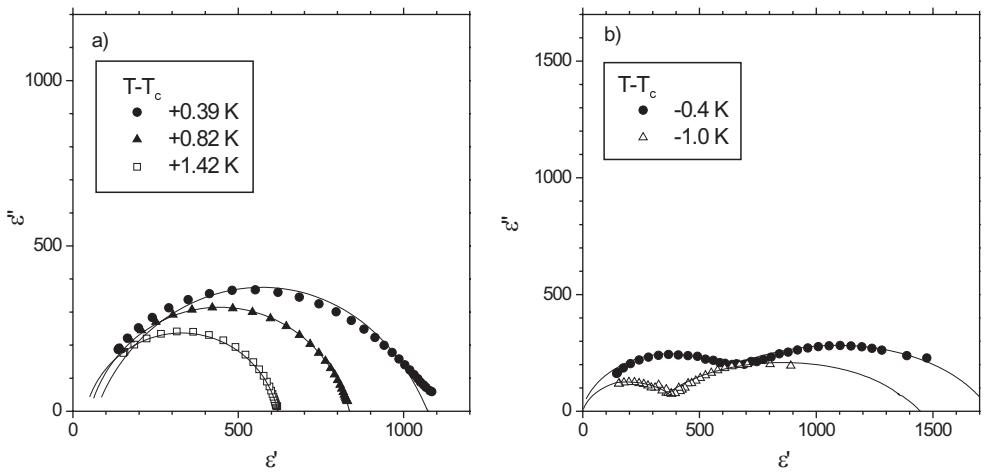

Figure 5. Cole–Cole diagrams in the paraelectric phase (a) and the ferroelectric phase (b) for a few temperatures in the vicinity of the Curie point.

is interpreted as due to a more complex character of relaxation of the ferroelectric phase. The estimated characteristic time τ_0 of the paraelectric phase is 170×10^{-12} s and is about three orders of magnitude longer than the relaxation times of the ferroelectrics with hydrogen bonds [20–23]. This means that hydrogen bonds do not play an important role in the ferroelectric phase transition of $PyReO_4$.

3.3. The nature of ferroelectricity in $PyReO_4$

For $PyReO_4$ the origin of the ferroelectricity may be related to the displacement of two ionic sublattices and/or to the ordering of the dipole moments of both ions. There is no shift of the Re-atom position at the phase transition going from the paraelectric to the ferroelectric phase (see table 2(a)), which excludes the possibility of the displacive type of ferroelectricity in $PyReO_4$.

The pyridinium cation is asymmetric and carries a dipole moment. However, in the paraelectric centrosymmetric crystal phase at 350 K, the cation is disordered, exhibits *mm* symmetry and undergoes reorientations about the pseudo-sixfold axis, as was confirmed by NMR measurements [3]. Therefore, the averaged dipole moment is equal to zero. The same zero value of the dipole moment in the paraelectric phase is shown by the symmetrical ReO_4^- anion.

In the ferroelectric phase the pyridinium cation is still disordered and, like in the paraelectric phase, the cation reorients and the position of the N atom cannot be defined. However, the *m* site symmetry and quite different reorientations of the cation [3] indicate the existence a non-zero dipole moment of pyridinium cation. The same phenomenon occurs for the ReO_4^- anions. They are distorted from the regular tetrahedron, losing one *m*-symmetry plane, and the difference in Re–O bond length of the order of 0.1 Å can induce non-negligible dipole moments. These dipole moments on average are directed along the ferroelectric twofold polar axis.

So we can conclude that the ferroelectricity originates from the change in disorder of the dipoles of the pyridinium cations as well as from the appearance of the dipole of the distorted ReO_4^- anion. A relatively high value of τ_0 for $PyReO_4$ also confirms that the ferroelectric

phase transition is of the order–disorder type. The occurrence of the critical slowing down at such low frequencies is related to the reorientations of the pyridinium cation having a large moment of inertia.

The phase transition index is defined as the ratio of the order of the paraelectric point group divided by the order of the ferroelectric point group [24] and is equal to 2 for the $mmm \overset{336\ \mathrm{K}}{\Longrightarrow} mm2$ ferroelectric phase transition in $PyReO_4$. This means that there are two kinds of ferroelectric domain in $PyReO_4$, and the crystals of $PyReO_4$ belong to the class of one-axis ferroelectrics.

4. Conclusions

$PyReO_4$ was found to undergo a series of structural phase transitions characterized by the following changes in the symmetry: $Cmcm \overset{336\mathrm{K}}{\Longrightarrow} Cmc2_1 \overset{250\ \mathrm{K}}{\Longrightarrow} Pbca$, and the structures of the three phases at 350 K, 293 K and 220 K were determined by x-ray diffraction investigations. The three phases are orthorhombic with space groups $Cmcm$, $Cmc2_1$ and $Pbca$ respectively. In the two high-temperature phases at 293 K and 350 K, only the pyridinium cations are disordered, while the ReO_4^- ions are well ordered. The N-atom position cannot be determined in these phases. In the low-temperature phase the pyridinium cations as well as the ReO_4^- anions are ordered. Because of the very large absorption coefficient of $PyReO_4$, all of the geometrical parameters, such as bond lengths and valency angles, are not very accurate, especially for the two high-temperature phases. The critical slowing down phenomenon was observed at the ferroelectric phase transition at frequencies of the order of a few MHz. For the paraelectric phase the dynamics of the critical slowing down can be described as a relaxation mode with a single relaxation time. The occurrence of the relaxation mode at relatively low frequencies testifies to the order–disorder character of the ferroelectric phase transition. The nature of the ferroelectricity of $PyReO_4$ is related to the change of disorder of the pyridinium cation as well as to the appearance of the dipole moment of ReO_4^- anions. $PyReO_4$ belongs to the single-axis class of ferroelectrics.

Acknowledgment

This work was supported by the State Committee for Scientific Research under Grant No 2P03B15615.

References

[1] Czarnecki P, Nawrocik W, Pająk Z and Wąsicki J 1994 *Phys. Rev.* B **49** 1511
[2] Czarnecki P, Nawrocik W, Pająk Z and Wąsicki J 1994 *J. Phys.: Condens. Matter* **6** 4955
[3] Wąsicki J, Czarnecki P, Pająk Z, Nawrocik W and Szczepański W 1997 *J. Chem. Phys.* **107** 576
[4] Pająk Z, Czarnecki P, Wąsicki J and Nawrocik W 1998 *J. Chem. Phys.* **109** 6420
[5] Burfoot J C and Taylor G W 1979 *Polar Dielectrics and Their Applications* (London: MacMillan)
[6] Wąsicki J, Nawrocik W, Pająk Z, Natkaniec I and Belushkin A V 1989 *Phys. Status Solidi* a **114** 497
[7] Kozak A, Wąsicki J and Pająk Z 1996 *Phase Transitions* **57** 153
[8] Wąsicki J, Pająk Z and Kozak A 1990 *Z. Naturf.* a **45** 33
[9] Czarnecki P, Wąsicki J, Pająk Z, Goc R, Małuszyńska H and Habryło S 1997 *J. Mol. Struct.* **404** 175
[10] Czarnecki P, Katrusiak A, Szafraniak I and Wąsicki J 1998 *Phys. Rev.* B **57** 3326
[11] Hartl H 1975 *Acta Crystallogr.* B **31** 1781
[12] Dutkiewicz G and Pająk Z 1998 *Z. Naturf.* b **53** 1323
[13] Sheldrick G 1986 *SHELXS-86 Program for Crystal Structure Determination* University of Göttingen
[14] Sheldrick G 1998 *SHELXL-98 Program for crystal Structure Determination* University of Göttingen

[15] Flack H D 1983 *Acta Crystallogr.* A **39** 876
[16] Jeffrey G A and Saenger W 1992 *Hydrogen Bonding in Biological Structures* (Berlin: Springer) pp 20–21
[17] Alexandru H V and Berbecara C A 1997 *Ferroelectrics* **202** 173
[18] Giletta F 1972 *Phys. Status Solidi* a **12** 143
[19] Landau L D and Khalatnikov I M 1954 *Dokl. Acad. Nauk SSSR* **46** 469
[20] Sekine A, Sumita M, Osaka T and Makita Y 1998 *J. Phys. Soc. Japan* **57** 4004
[21] Baran J, Śledź M, Jakubas R and Bator G 1997 *Phys. Rev.* B **55** 169
[22] Komukae M and Makita Y 1986 *J. Phys. Soc. Japan* **54** 4359
[23] Kanda E, Tamaki A and Fujimuru T 1982 *J. Phys. C: Solid State Phys.* **15** 3401
[24] Boccara N 1968 *Ann. Phys., NY* **47** 40